ELSEVIER

Chemical Engineering Journal 137 (2008) 568–578

Chemical Engineering Journal

www.elsevier.com/locate/cej

Modeling and analysis of autothermal reforming of methane to hydrogen in a fixed bed reformer

M.H. Halabi [a], M.H.J.M. de Croon [a], J. van der Schaaf [a], P.D. Cobden [b], J.C. Schouten [a,*]

[a] *Laboratory of Chemical Reactor Engineering, Department of Chemical Engineering & Chemistry, Eindhoven University of Technology, P.O. Box 513, 5600 MB Eindhoven, The Netherlands*

[b] *Energy Research Center of the Netherlands, P.O. Box 1, 1755 ZG Petten, The Netherlands*

Received 29 March 2007; received in revised form 11 May 2007; accepted 15 May 2007

Abstract

This paper presents a performance analysis for the autothermal reforming process of methane in a fixed bed reformer for hydrogen production. The process is simulated using a 1-D heterogeneous reactor model under small-scale conditions. The model accounts for mass and thermal dispersion in the axial direction, axial pressure distribution, and interfacial and intraparticle transport. The process performance under dynamic and steady state conditions is analyzed with respect to key operational parameters: temperatures of gas feed and catalyst bed, oxygen/carbon and steam/carbon ratios, gas hourly space velocity (GHSV), and feed contaminations. The influence of these parameters on gas temperature, methane conversion, hydrogen yield and purity, and reforming efficiency is investigated. An optimal operational window of a GHSV range from 1050 to 14,000 h^{-1}, steam/carbon molar ratio of 4.5–6.0, and oxygen/carbon molar ratio of 0.45–0.55 is obtained to achieve a high conversion level of 93%, hydrogen purity of 73% on dry basis, thermal reformer efficiency of 78%, and a yield of 2.6 mole hydrogen per 1 mole of methane fed. The simulation studies are performed using gas feed temperature and pressure of 500 °C and 1.5 bar, respectively.

Keywords: Methane autothermal reforming; Hydrogen production; Mathematical modeling; Fixed bed reactor

1. Introduction

Hydrogen is a major feedstock in many chemical and petrochemical industries and well perceived as a pollution-free primary energy carrier for future transportation fuel as well as electricity generation. The recent surge in demand for small-scale, cheap, and efficient hydrogen production is driven by the high interest in the application of fuel cells for electricity generation [1–3]. Fuel cells offer a promising path for hydrogen based energy systems as clean, flexible, and efficient devices utilized in either stationary or portable power generation applications and in transportation [3,4].

A typical gas mixture feed to a fuel cell can be obtained by converting the hydrocarbon fuel first into synthesis gas in a reformer. For a proton exchange membrane fuel cell, the gas feed must be purified in a water gas shift reactor where CO is converted into CO_2 and additional hydrogen is obtained. The remaining traces of CO have to be removed further, for instance by selective oxidation, before the final gas mixture is fed to the anode side of the fuel cell.

A complete transition towards hydrogen as a standard energy carrier within the next decade is unlikely, due to the current difficulties in its economically and technically feasible production routes and storage. The ultimate goal towards hydrogen economy is to use renewable energy for hydrogen production. Thus, reforming fuel for hydrogen production is solely an intermediate solution. Nevertheless, the ongoing research on hydrogen technology may significantly improve the energy efficiency [5,6].

Methane reforming is currently a well-established technology and has been the most important industrial process for the production of hydrogen and/or synthesis gas in the manufacture of ammonia, methanol, and other chemicals. This technology has been adequately reviewed [7–13]. The major reforming processes include steam reforming (SR), partial oxidation reforming (POX), catalytic partial oxidation (CPO), and autothermal reforming (ATR).

* Corresponding author. Tel.: +31 40 274 3088; fax: +31 40 244 6653.
E-mail address: j.c.schouten@tue.nl (J.C. Schouten).

1385-8947/$ – see front matter © 2007 Elsevier B.V. All rights reserved.
doi:10.1016/j.cej.2007.05.019

Nomenclature

a_v	external catalyst surface area per unit volume of catalyst bed (m^2/m^3)
C_i	concentration of species i in the gas phase (mol/m^3)
$C_{i,s}$	concentration of species i in the solid phase (mol/m^3)
$C_{p,bed}$	specific heat of the catalyst bed (J/(kg K))
C_{pg}	specific heat of the fluid (J/(kg K))
D_i	effective diffusion coefficient (m^2/s)
D_m	average molecular diffusivity (m^2/s)
D_z	axial dispersion coefficient (m^2/s)
d_p	catalyst particle diameter (m)
E_j	activation energy of reaction j (J/mol)
G_s	gas mass flow velocity (kg/(m^2 s))
ΔH_i	heat of adsorption of species i (J/mol)
ΔH_i^C	heat of adsorption of combusting species i (J/mol)
$\Delta H_{298\,K}$	heat of reaction of at STP (kJ/mol)
h_f	gas to solid heat transfer coefficient (W/(m^2 s))
j_D	Chilton–Colburn factor for mass transfer
j_H	Chilton–Colburn factor for heat transfer
$k_{g,i}$	gas to solid mass transfer coefficient of component i ($m^3/(m^2$ s))
k_j	temperature dependent kinetic rate constant of reaction j
k_{oj}	reference temperature dependent kinetic rate constant of reaction j
K_j	thermodynamic equilibrium constant of reaction j
K_{oi}	reference adsorption constant of species i
K_i	adsorption constant of species i
K_{oi}^C	reference adsorption constant of combusting species i
K_i^C	adsorption constant of combusting species i
K_D	parameter corresponding to the viscous loss term (Pa s/m^2)
K_V	parameter corresponding to the kinetic loss term (Pa s^2/m^3)
LHV_{H_2}	lower heating value of H_2 (MJ/kmol)
LHV_{CH_4}	lower heating value of CH_4 (MJ/kmol)
p_i	partial pressure of gas species i (bar)
P	total gas pressure (bar)
Pr	Prandtl number
r_i	rate of consumption or formation of species i (mol/(kg_{cat} s))
R_j	rate of reaction j (mol/(kg_{cat} s))
R	universal gas constant (J/mol K)
Re	Reynolds number
Sc_i	Schmitt number
T	gas phase temperature (K)
T_s	solid catalyst temperature (K)
t	time (s)
u	superficial gas flow velocity ($=\varepsilon_b u_{inst}$) (m/s)
u_{inst}	interstitial gas velocity (m/s)
Y_i	dry mole fraction of species i (mol/mol)
z	axial dimension (m)

Greek letters

Ω	dominator term in the reaction kinetics
ε_b	packing bed porosity
η_j	effectiveness factor of reaction j
λ_g	average gas thermal conductivity (W/m K)
λ_s	solid thermal conductivity (W/m K)
λ_z^f	effective thermal conductivity (W/m K)
μ_g	average gas viscosity (kg/(m s))
ρ_{bed}	density of the catalyst bed (kg/m^3)
ρ_{cat}	density of the catalyst pellet (kg/m^3)
ρ_f	density of the fluid (kg/m^3)
ψ	particle shape factor (for spherical particles, $\psi = 1$)

SR is a highly endothermic process and therefore demands an efficient heat supply to the system. It is usually operated in a temperature range of 850–950 °C on Ni-based catalyst. It is a very energy- and capital-intensive process although the present technology approaches 90% of the maximum thermodynamic efficiency [14]. However, steam reforming is economically unattractive option for low-volume and low-pressure hydrogen production [6,12].

POX uses pure oxygen and achieves H_2 to CO ratios from 1.6 to 1 in the product syngas. CPO uses a catalyst that permits flameless partial combustion to H_2 and CO [13]. Conventional ATR uses a partial oxidation burner followed by a catalyst bed with natural gas, steam and oxygen to produce syngas with H_2 to CO ratios of 2 to 1 [6]. CPO typically operates at low steam/carbon ratio (S/C from 0 to 1), while ATR operates at relatively higher steam load (S/C > 1). In CPO, the catalyst bed temperatures tend to be higher than ATR and thus higher reaction rates and consequently a higher space velocity is possible even the syngas yield is somewhat lower than ATR [2]. However, premixing and preheating is more straightforward because there is no steam is fed to the process. Currently, CPO and ATR require added oxygen which increases the costs for low volume hydrogen production. In both processes, the target is to achieve the thermodynamic equilibrium composition, which is governed by feed conditions (composition, temperature), pressure, and heat loss. These factors must be optimized to maximize the syngas yield, and to minimize the hydrocarbon slip.

Because of thermodynamic reversibility of the SR reactions and the POX reactions, limits are imposed on the maximum methane conversion and hydrogen yield that can be attained in conventional fixed bed large-scale units. Therefore, a strong necessity in such technologies is to include further purification units of hydrogen using shift reactors, CO_2 separation units, preferential CO oxidation units (PROX), and pressure-swing absorption units (PSA). These operational units, particularly the PSA, are highly cost intensive and inconvenient for small-scale applications such as onboard fuel cells. Extensive thermody-

namic calculations have been performed on ATR of natural gas to analyze the equilibrium product composition and the influence of the natural gas composition on optimizing hydrogen yield and minimizing CO co-generation [15–17].

The catalytic ATR has received much attention in research during the recent years as a viable process for hydrogen generation for fuel cell systems [6,11,12]. It offers advantages of small unit size and lower operational temperature, easier startup, and wider choice of materials. Moreover, it has a higher energy efficiency compared to SR or POX. ATR has major advantages over other reforming alternatives mainly for low energy requirements, high GHSV (at least one order of magnitude relative to SR), and lower process temperature than POX, higher H_2/CO ratio, and easily regulated H_2/CO ratio by the inlet gas composition.

Although ATR has an interesting potential in industrial application, there has been only a limited amount of work reported in the field of reactor design and simulation [18]. In this paper, the autothermal reforming of methane is optimized in terms of fuel conversion, reforming efficiency, and H_2 purity and yield in a fixed bed reactor with a mathematical modeling approach at small-scale conditions. The process performance under dynamic and steady state conditions is analyzed with respect to major operational parameters: temperatures of gas feed and catalyst bed, oxygen/carbon and steam/carbon ratios, gas feed space velocity, and feed contaminations. An optimal operational window of GHSV, oxygen/carbon ratio, and steam/carbon ratio is characterized under relatively mild conditions of temperature and pressure. The influence of the reforming-oxidation kinetic model and reactor conditions on catalyst and gas temperatures is discussed. Furthermore, the formation of undesired hot spots in the fixed bed reformer as a function of oxygen partial pressure can be predicted with the model. Special attention must be paid to this point in the design and construction stage of such reactor.

2. Autothermal reforming of natural gas

ATR combines the effects of both the endothermic steam reforming and the exothermic partial oxidation by feeding the fuel together with the oxidant (air fed or oxygen fed) and steam over a catalyst in a fixed bed reactor.

2.1. ATR reactions

In a reforming process of natural gas, many reactions are likely to occur. If we consider that methane is the major dominating species in natural gas, the following set of reactions shown in Table 1 will be involved. The first four reactions are considered as the prevailing reaction routes in the autothermal reforming process. The water gas shift reaction tends to influence the final H_2/CO ratio depending on the feed S/C ratio. At high operational temperature, the reaction will favor production of CO instead of H_2; that is the reason why a large S/C ratio is used in methane reforming.

It is also theoretically possible to reform methane with CO_2, this is known as dry reforming as represented in reaction (7). The catalysis research for such a reforming route of methane is still very challenging and the formation of acceptable amounts of syngas or H_2 via this route alone does not appear feasible yet [6].

Table 1
Autothermal reforming reactions

	Reaction	$\Delta H_{298\,K}$ (kJ/mol)
R_1. Steam reforming	$CH_4 + H_2O \leftrightarrow CO + 3H_2$	206.2
R_2. Steam reforming	$CH_4 + 2H_2O \leftrightarrow CO_2 + 4H_2$	164.9
R_3. Water gas shift	$CO + H_2O \leftrightarrow CO_2 + H_2$	−41.1
R_4. Total combustion	$CH_4 + 2O_2 \leftrightarrow CO_2 + 2H_2O$	−802.7
R_5. Partial oxidation	$CH_4 + \frac{1}{2}O_2 \leftrightarrow CO + 2H_2$	−36
R_6. Partial combustion	$CH_4 + O_2 \leftrightarrow CO_2 + 2H_2$	−71
R_7. Dry reforming	$CH_4 + CO_2 \leftrightarrow 2CO + 2H_2$	247
R_8. Boudouard reaction	$2CO \leftrightarrow C + CO_2$	−172
R_9. Decomposition	$CH_4 \leftrightarrow C + 2H_2$	75

The reforming reactions may also be associated with coke formation in some cases as in reactions (8) and (9). The coke formation reactions are definitely undesired routes due to the reduced process efficiency attained, catalyst deactivation, corrosion of material of construction and unfavorable reactor cleaning. However, coke formation is usually suppressed by higher temperatures, and high O/C and S/C operational ratios [1,4,15]. A similar set of reactions is expected to occur with ethane and other hydrocarbons in the feed.

2.2. Thermal neutrality condition of ATR

The overall ATR reforming of methane is ideally expressed by the following reaction equation:

$$CH_4 + x(O_2) + (2-2x)H_2O \Leftrightarrow CO_2 + (4-2x)H_2 \quad (1)$$

where x is the O/C molar ratio. This ratio is the key stoichiometric parameter that determines the theoretical S/C molar ratio required to convert CH_4 into CO_2 and H_2, the maximum H_2 yield, and the heat of reaction at adiabatic conditions at a defined temperature. Autothermicity of the reaction can be theoretically attained when the net adiabatic heat of reaction is zero:

$$\Delta H_T = \sum_i \nu_{i(x)} H_{i(T)} = 0 \quad (2)$$

However, due to heat transfer losses through the reactor walls, the operating O/C ratio should be slightly higher than the stoichiometric ratio to account for any heat loss or to raise the gas temperature to control the product composition and to limit coke formation.

3. Mathematical model

A 1-D heterogeneous model is constructed to investigate the ATR process behavior at dynamic and steady state conditions in a fixed bed reformer. The major assumptions in the model can be listed as follows:

1. ideal gas behavior;
2. adiabatic operation;
3. mass axially dispersed plug-flow conditions are considered with negligible radial gradients;

4. thermal dispersion in the axial direction is also considered with negligible radial gradients;
5. concentration and temperature gradients in the radial direction are ignored;
6. no temperature gradient in the catalyst particles;
7. six reactive species (CH_4, O_2, CO, CO_2, H_2, H_2O) and one inert component (N_2) are involved in the model;
8. no homogenous gas phase reactions are considered as the temperatures are lower than 600 °C;
9. uniform particle size;
10. constant bed porosity.

3.1. Reaction kinetic model

To reduce the complexity of the mathematical model development and solution, only the reactions with significant rates will be considered. Among the possible set of reactions previously discussed, the two steam reforming reactions R_1 and R_2, water gas shift R_3, and the total combustion reaction R_4 prove to have significant rates [15]. Therefore, the partial oxidation reaction R_5, the partial combustion reaction R_6, the dry reforming reaction R_7, the Boudouard reaction R_8, and the decomposition reaction R_9 are ignored in this modeling study. There is a large number of kinetic models for steam reforming and water-gas shift reactions in literature. The model of Xu and Froment [19] over Ni-based catalyst is considered to be more general and has been extensively tested under labscale conditions [20]. It is investigated on a temperature range from 500 to 575 °C. The kinetic model of Trimm and Lam [21] is considered as a rigorous study for methane combustion. The kinetic rate expression developed in their model at 557 °C is adopted for the methane combustion reaction in this work. However, since it was derived over supported Pt-based catalyst, the model adsorption parameters are adjusted for Ni-based catalyst [22]. The combined model for the kinetic rate equations of ATR is given in Table 2. The reaction equilibrium constants and Arrhenius kinetic parameters are listed in Table 3. Van't Hoff parameters for species adsorption are given in Table 4.

Table 2
ATR kinetic reaction model

Reaction rate equation	
$R_1 = \frac{k_1}{p_{H_2}^{2.5}}\left(p_{CH_4}p_{H_2O} - \frac{p_{H_2}^3 p_{CO}}{K_I}\right)\times\frac{1}{\Omega^2}$	(3)
$R_2 = \frac{k_2}{p_{H_2}^{3.5}}\left(p_{CH_4}p_{H_2O}^2 - \frac{p_{H_2}^4 p_{CO_2}}{K_{II}}\right)\times\frac{1}{\Omega^2}$	(4)
$R_3 = \frac{k_3}{p_{H_2}}\left(p_{CO}p_{H_2O} - \frac{p_{H_2}p_{CO_2}}{K_{III}}\right)\times\frac{1}{\Omega^2}$	(5)
$R_4 = \frac{k_{4a}p_{CH_4}p_{O_2}}{(1+K^C_{CH_4}p_{CH_4}+K^C_{O_2}p_{O_2})^2} + \frac{k_{4b}p_{CH_4}p_{O_2}}{1+K^C_{CH_4}p_{CH_4}+K^C_{O_2}p_{O_2}}$	(6)
$\Omega = 1 + K_{CO}p_{CO} + K_{H_2}p_{H_2} + K_{CH_4}p_{CH_4} + K_{H_2O}\frac{p_{H_2O}}{p_{H_2}}$	(7)

The rate of consumption or formation of species i, r_i (mol/(kg_{cat} s)) is determined by summing up the reaction rates of that species in all the reactions R_j (mol/(kg_{cat} s)). Effectiveness factors η_j are used to account for the intraparticle transport limitation [23–25]. Therefore, the reaction rate of each species becomes:

$$r_{CH_4} = -\eta_1 R_1 - \eta_2 R_2 - \eta_4 R_4 \quad (8\text{-a})$$

$$r_{O_2} = -2\eta_4 R_4 \quad (8\text{-b})$$

$$r_{CO_2} = \eta_2 R_2 + \eta_3 R_3 + \eta_4 R_4 \quad (8\text{-c})$$

Table 3
Reaction equilibrium constants and Arrhenius kinetic parameters

Reaction, j (see Table 1)	Equilibrium constant, K_j	k_{oj} (mol/(kg_{cat} s))	E_j (J/mol)
1	$K_I = \exp\left(\frac{-26830}{T_s} + 30.114\right)$ (bar^2)	1.17×10^{15} bar$^{0.5}$	240,100
2	$K_{II} = K_I \cdot K_{III}$ (bar^2)	2.83×10^{14} bar$^{0.5}$	243,900
3	$K_{III} = \exp\left(\frac{4400}{T_s} - 4.036\right)$	5.43×10^{5} bar^{-1}	67,130
4		8.11×10^{5} bar^{-2}	86,000
		6.82×10^{5} bar^{-2}	86,000
$k_j = k_{oj}\times\exp\left(\frac{-E_j}{RT}\right)$			

Table 4
Van't Hoff parameters for species adsorption

	K_{oi} (bar^{-1})	ΔH_i (J/mol)	K^C_{oi} (bar^{-1})	ΔH^C_i (J/mol)
CH_4	6.65×10^{-4}	−38,280		
CO	8.23×10^{-5}	−70,650		
H_2	6.12×10^{-9}	−82,900		
H_2O	1.77×10^{5} bar	88,680		
CH_4 (combustion)			1.26×10^{-1}	−27,300
O_2 (combustion)			7.78×10^{-7}	−92,800
$K_i = K_{oi}\times\exp\left(\frac{-\Delta H}{RT}\right)$				
$K^C_i = K^C_{oi}\times\exp\left(\frac{-\Delta H^C_i}{RT}\right)$				

Table 5
Reactor simulation model with corresponding boundary and initial conditions

Mass and energy balances in the gas phase	$\varepsilon_b \frac{\partial C_i}{\partial t} + \frac{\partial (uC_i)}{\partial z} + k_{g,i} a_v (C_i - C_{i,s}) = \varepsilon_b D_Z \frac{\partial^2 C_i}{\partial z^2}$	(9)
	$\varepsilon_b \rho_f C_{pg} \frac{\partial T}{\partial t} + u \rho_f C_{pg} \frac{\partial T}{\partial z} = h_f a_v (T_s - T) + \lambda_z^f \frac{\partial^2 T}{\partial z^2}$	(10)
Mass and energy balances in the solid phase	$k_{g,i} a_v (C_i - C_{i,s}) = (1 - \varepsilon_b) \rho_{cat} r_i$	(11)
	$\rho_{bed} C_{p,bed} \frac{\partial T_s}{\partial t} + h_f a_v (T_s - T) = \rho_{cat} (1 - \varepsilon_b) \sum -\Delta H_{rxn,j} \eta_j R_j$	(12)
	Note: rate of accumulation of the concentration in the solid particle ($C_{i,s}$) is ignored, due to small particle size, see [26].	
Pressure drop	$\frac{\partial P}{\partial z} = -K_D u - K_V u^2$	(13)
Boundary conditions	At the reformer inlet $z = 0.0$	
	$C_i = C_{i,o} \quad T = T_o \quad T_s = T_{s,o} \quad P = P_o$	(14)
	At the reformer exit $z = L$	
	$\frac{\partial C_i}{\partial z} = 0 \quad \frac{\partial T}{\partial z} = 0 \quad \frac{\partial T_s}{\partial z} = 0$	(15)
Initial conditions	$C_i = C_{i,o} \quad T = T_o \quad T_s = T_{s,o}$	(16)

$$r_{H_2O} = -\eta_1 R_1 - 2\eta_2 R_2 - \eta_3 R_3 + 2\eta_4 R_4 \quad (8\text{-d})$$

$$r_{H_2} = 3\eta_1 R_1 + 4\eta_2 R_2 + \eta_3 R_3 \quad (8\text{-e})$$

$$r_{CO} = \eta_1 R_1 - \eta_3 R_3 \quad (8\text{-f})$$

where $\eta_1 = 0.07$, $\eta_2 = 0.06$, $\eta_3 = 0.7$, $\eta_4 = 0.05$ [23].

3.2. Governing equations

The mathematical model developed is typically composed of mass and energy balance equations in the gas and the solid phases as shown in Table 5.

Pressure drop along the axial direction in the fixed bed is described by the Ergun equation [27]. K_D and K_V are parameters corresponding to the viscous and kinetic loss terms, respectively, and given in Table 6. The axial dispersion coefficient to account for the non-ideal flow and local mixing at turbulent velocities plus the diffusive flow is estimated using the equation of Edwards and Richardson [28], see Table 6. The axial thermal effective conductivity of the bed shown in Table 6 is determined from Ref. [29], see also [30–33]. The gas and catalyst temperatures are initially equal to the feed temperature at the start up conditions. Therefore, the catalyst bed is heated up to the feed temperature. The initial and boundary conditions are summarized in Table 5.

3.3. Gas properties and transport coefficients

Gas properties such as the fluid density, heat capacity, thermal conductivity, and viscosity are naturally functions of temperature as well as of composition, and they are changing along the reformer length and might vary with time. Temperature and composition dependent expressions are employed in the model to calculate the gas properties throughout the reactor [34,35]. However, average values are only used to calculate the gas viscosity and thermal conductivity, the solid thermal conductivity, and the bed heat capacity [37]. The mass transfer coefficient from gas to solid, $k_{g,i}$, is calculated from the Chilton–Colburn factor, j_D, for mass transfer [36], see also [35]. The heat transfer coefficient, h_f, is also determined from the Chilton–Colburn factor, j_H [36]. The transport coefficients are presented in Table 6.

Table 6
Empirical correlations employed in the model

Semi-empirical relations for K_D and K_V [27]

$$K_D = \frac{150 \mu_g (1 - \varepsilon_b)^2}{d_p^2 \varepsilon_b^3} \ (\text{Pa s/m}^2); \qquad K_V = \frac{1.75 (1 - \varepsilon_b) \rho_f}{d_p \varepsilon_b^3} \ (\text{Pa s}^2/\text{m}^3)$$

Mass axial dispersion coefficient [28]

$$D_Z = 0.73 D_m + \frac{0.5 u d_p}{1 + 9.49 D_m / u d_p}$$

Effective thermal conductivity [29]

$$\frac{\lambda_z^f}{\lambda_g} = \frac{\lambda_z^{f,o}}{\lambda_g} + 0.75 \cdot Pr \cdot Re_p \ , \qquad \frac{\lambda_z^{f,o}}{\lambda_g} = \varepsilon_b + \frac{1 - \varepsilon_b}{0.139 \varepsilon_b - 0.0339 + (2/3) \lambda_g / \lambda_s}$$

Mass transfer coefficient [36]

$$k_{g,i} = j_{D,i} Re \cdot Sc_i{}^{1/3} \frac{D_i}{d_p}, \qquad \varepsilon_b j_{D,i} = 0.765 Re^{-0.82} + 0.365 Sc_i{}^{-0.398}, \qquad Re = \frac{\rho_f u d_p}{\mu}, \qquad Sc_i = \frac{\mu}{\rho_f D_i} \quad 0.01 < Re < 1500, \quad 0.6 < Sc < 7000, \quad 0.25 < \varepsilon_b < 0.96$$

Heat transfer coefficient [36]

$$h_f = j_H \frac{C_{pg} G_s}{Pr^{2/3}}, \quad j_H = 0.91 Re^{-0.51} \psi, \quad 0.01 < Re < 50, \quad j_H = 0.61 Re^{-0.41} \psi, \quad 50 < Re < 1000, \quad Pr = \frac{C_{pg} \mu_g}{\lambda_g}$$

Table 7
Reactor parameters, operating conditions, and average gas properties used in the model simulations

	Unit	Value
Reactor length	m	0.4
Gas feed temperature	°C	500
Catalyst temperature	°C	500
Pressure	bar	1.5
Solid density [22]	kg/m^3	1870
Bed voidage	–	0.4
Particle diameter	m	2×10^{-3}
Gas mass flow velocity	kg/(m^2 s)	0.15
Steam/carbon molar ratio	–	6.0
Oxygen/carbon molar ratio	–	0.45
Average gas properties		
Molecular diffusivity, D_m	m^2/s	1.6×10^{-5}
Gas viscosity, μ_g	kg/(m s)	0.031×10^{-3}
Gas thermal conductivity, λ_g	W/(m K)	0.0532
Solid thermal conductivity, λ_s	W/(m K)	13.8
Bed heat capacity, $C_{p,bed}$ [37]	J/(kg K)	850
LHV_{H_2}	MJ/kmol	240
LHV_{CH_4}	MJ/kmol	800

3.4. Numerical solution

The mathematical model consisting of coupled partial differential and algebraic equations is implemented and solved in gPROMS modeling environment (Process Systems Enterprise Ltd.). Backward difference of first order is used as a spatial discretization method over a uniform grid of 100 intervals. The integration over the time domain is performed by the DAE integrator based on the variable time step of the backward differentiation formula. Reactor parameters, operating conditions, and average gas properties used globally throughout this simulation study are listed in Table 7.

4. Results and discussion

The most recent work for modeling of autothermal reforming of CH_4 for H_2 production by Hoang and Chan [18], presents potential operating conditions for high CH_4 conversion and H_2 purity (on dry basis) at a S/C ratio of 1 and an air/carbon ratio (A/C) of 3.5 (equivalent to an O/C ratio of 0.74). They obtained a conversion of 98% and H_2 purity and yield of 42% and 1.9%, respectively. However, a further insight in the reforming process can generate improved operation performance in terms of reforming efficiency, and H_2 purity and yield using higher S/C ratios to boost the reaction selectivity towards H_2 production and lowering the air or oxygen to carbon ratios to merely provide sufficient energy for the endothermic reforming reactions.

Fig. 1 shows the composition distribution during autothermal reforming at different temperatures at thermodynamic equilibrium at a pressure of 1.5 bar and molar ratios of S/C and O/C of 6 and 0.45, respectively. Higher CH_4 conversion is naturally favored at elevated temperatures. Conversion levels greater than 96% can be achieved at temperatures above 500 °C. However, the H_2 purity (defined as mole fraction of H_2 on dry basis, $Y_{dry}(H_2)$) obtained is gradually increasing with temperature until it reaches a maximum value of 74.1% at 500 °C, beyond which it starts to slightly decrease at higher temperatures and no further improvement can be attained. This is contributed to the fact that equilibrium between CO and CO_2 tends to favor the reverse water gas shift reaction and the equilibrium conditions are disturbed resulting in reduced H_2 concentration and increased CO concentration. Therefore, the gas feed temperature must be selected above 500 °C to give a maximum H_2 purity, taking into account that the adiabatic temperature rise of the reformer will already lead to a higher CH_4 conversion.

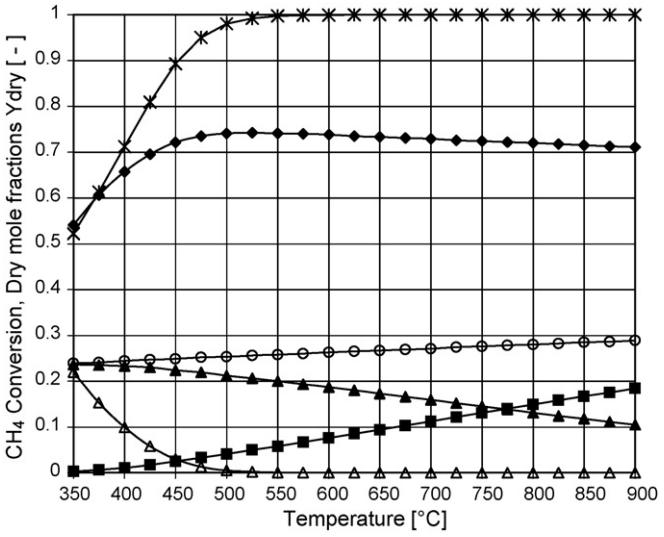

Fig. 1. ATR product gas composition at 1.5 bar, O/C = 0.45, S/C = 6 at thermodynamic equilibrium. (✱) CH_4 conversion; (♦) H_2; (■) CO; (▲) CO_2; (△) CH_4; (◯) CO + CO_2.

Fig. 2 shows the dynamic profiles of the gas temperature along the axial reformer direction at different times using the simulation parameters and conditions listed in Table 7 for gas feed flow, space velocity, pressure, and O/C and S/C ratios. The temperature is changing with time until it monotonically

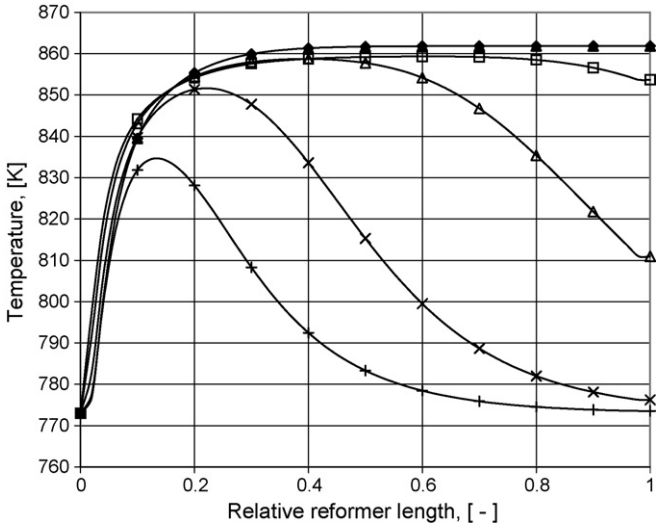

Fig. 2. Dynamic temperature profiles along the axial reformer direction at 500 °C, 1.5 bar, O/C = 0.45, S/C = 6. (+) 100 s; (×) 200 s; (△) 400 s; (□) 600 s; (♦) 1000 s; (▲) steady state.

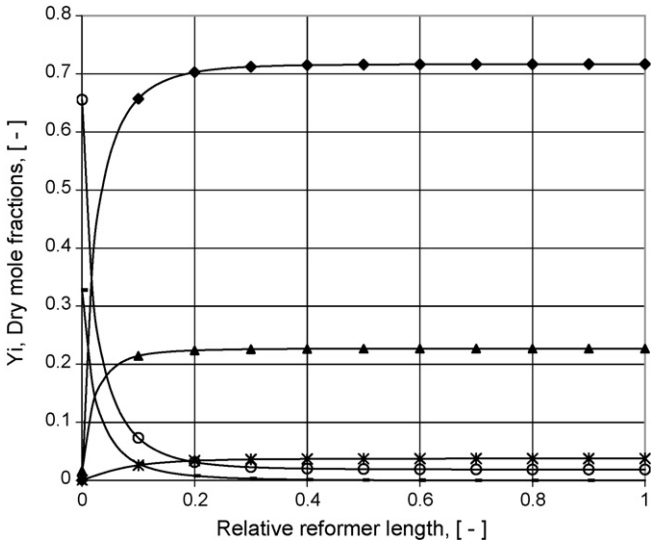

Fig. 3. Steady state composition profiles (on dry basis), at 500 °C, 1.5 bar, O/C = 0.45, S/C = 6. (♦) H_2; (▲) CO_2; (✱) CO; (◯) CH_4; (-) O_2.

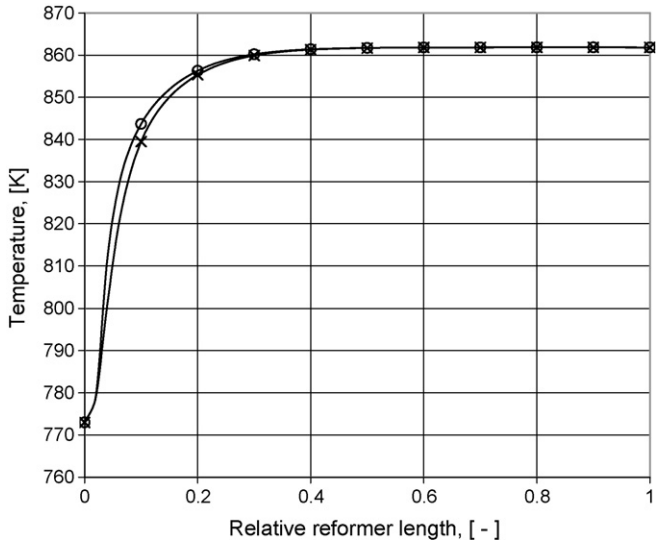

Fig. 4. Temperature profiles of bulk gas and solid catalyst at 500 °C, 1.5 bar, O/C = 0.45, S/C = 6. (✱) T_{gas}; (◯) $T_{catalyst}$.

approaches steady state conditions at 862 K in about 13 min with a maximum rise of 89 °C above the feed inlet temperature. The simulation curves show no peak value attained in the front part of the reformer and then are gradually flattening or even decreasing in the rear part as might be expected for the typical behavior of a catalytic partial oxidation reformer and even for a high O/C fed autothermal reformer [23,38,39]. This phenomenon is further discussed for high concentrations or high-pressure operation below.

The steady state composition profiles of the gas species on dry basis as a function of the axial reactor coordinate are given in Fig. 3. The H_2 purity obtained at the S/C ratio of 6, and O/C ratio of 0.45 is 73% with corresponding CH_4 conversion of 93%, H_2 yield of 2.6 mol H_2 produced/mol CH_4 fed, and thermal reforming efficiency of 78%. This thermal efficiency of the reforming process is defined as

$$\text{eff} = \frac{n_{H_2}, \text{mol H}_2 \text{ produced}}{n_{CH_4}, \text{mol CH}_4 \text{ fed}} \cdot \frac{\text{LHV}_{H_2}}{\text{LHV}_{CH_4}} \quad (17)$$

The front part of the reformer is obviously utilized to generate sufficient energy for the process, so that the oxidation reaction is dominating the front section while the rest of the reformer is dominated by the endothermic reforming reactions. Due to the high concentration of steam and relatively low concentration of oxygen in the reactor, the oxidation and the reforming reaction rates are almost of the same order of magnitude.

The wet concentration profiles show a peak for water in the first 10% of the reformer length as increased product concentration from the oxidation reaction. Thereafter, the water concentration decreases along the reformer length due to its consumption via the endothermic reforming reactions. However, feed oxygen is fully consumed by the catalytic oxidation reaction in the first 10% of the reformer.

Figs. 4–6 reveal how the ATR process behaves under the given simulated conditions in terms of heat transfer. Fig. 4 depicts the temperature profiles along the reformer at steady state in the gas and solid phases. It is evident that heat transfer is quite effective and the interfacial resistances between the catalyst and the gas are relatively small along the reformer, although the catalyst surface is about 11 °C higher in temperature than the bulk gas at the front section. This is due to the fact that heat of combustion generated in the catalyst is effectively transported to the bulk gas. The two profiles are almost identical after the first 20% of the reformer length. Similarly, the interfacial concentration gradients are found to be negligible due to effective mass transport in the gas film.

At relatively low O/C ratio of 0.45, S/C ratio of 0.6, a total pressure of 1.5 bar, and a GHSV of 3071 h^{-1} (residence time of 1.17 s, $G_s = 0.15$ kg/(m^2 s)), the monotonic behavior of the temperature profile is reasonably predicted as shown in Fig. 5.

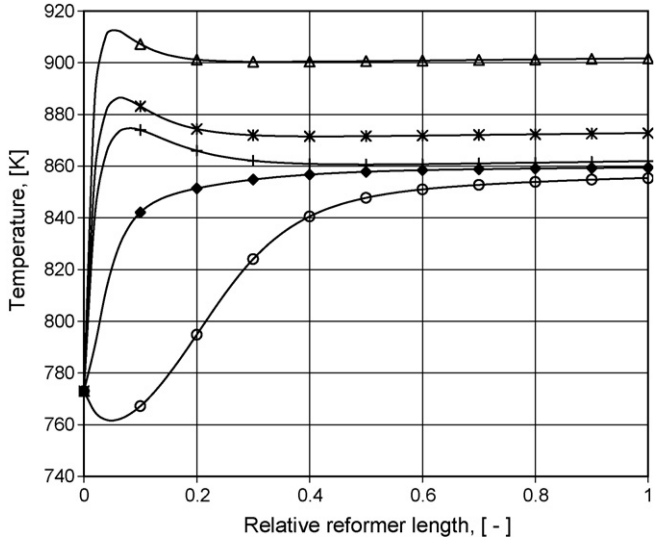

Fig. 5. Gas phase temperature profiles at different pressures and at 500 °C, O/C = 0.45, S/C = 6. (♦) $G = 0.15$ kg/(m^2 s), $P = 1.5$ bar; (◯) $G = 0.55$ kg/(m^2 s), $P = 1.5$ bar; (+) $G = 0.55$ kg/(m^2 s), $P = 4.5$ bar; (✱) $G = 0.55$ kg/(m^2 s), $P = 7.5$ bar; (△) $G = 0.55$ kg/(m^2 s), $P = 15$ bar.

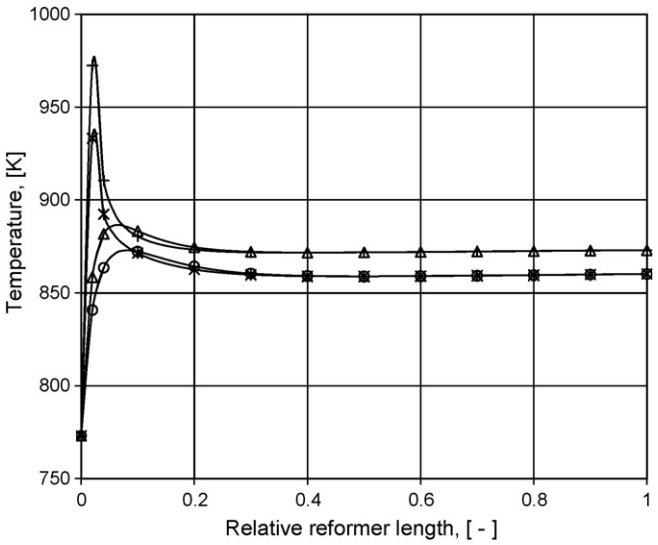

Fig. 6. Gas temperature profiles and spike-like catalyst temperature profiles at high concentration (pressure), at 500 °C, O/C = 0.45, S/C = 6. (◯) T_{gas}, $P = 4.5$ bar; (✱) $T_{catalyst}$, $P = 4.5$ bar; (△) T_{gas}, $P = 7.5$ bar; (+) $T_{catalyst}$, $P = 7.5$ bar.

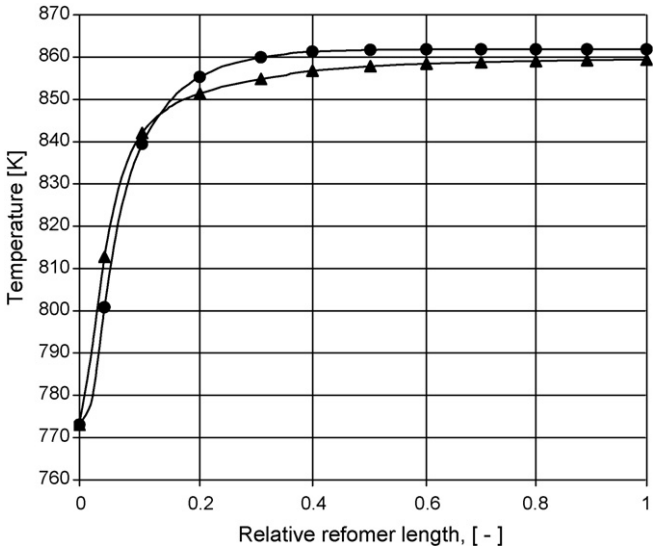

Fig. 7. Effect of axial thermal dispersion on ATR temperature profile. (●) With dispersion; (▲) no dispersion.

The figure shows two other important aspects of the process. At relatively low gas concentrations at low pressure of 1.5 bar and relatively high GHSV of 11,260 h^{-1} (residence time of 0.3 s, $G_s = 0.55$ kg/(m^2 s)), the oxidation kinetics [21] is somewhat slower than the reforming kinetics [19], which explains the dip in the temperature at the beginning of the reformer. Conversely, at higher operating pressure (higher concentrations), a temperature peak appears in the front part of the reformer (more than 150 °C gas temperature rise). Apparently, this is contributed to the fact that the oxidation rate becomes faster than the reforming rates at high pressure and lower temperatures. The peak gets sharper at higher pressures.

The catalyst temperature profiles at pressures of 4.5 and 7.5 bar are given in Fig. 6. Hot spot formation in the catalyst is observed due to the fast oxidation reaction at high oxygen partial pressures in the reformer front part. This phenomenon deserves considerable attention during reactor design, construction, and the distribution of the temperature sensing devices along the reactor length. Non-uniformity of oxygen distribution throughout the reactor may also escalate the occurrence of hot spots especially on an industrial scale operation. Hoang and Chan [40] have recently investigated the partial oxidation process using radial distribution oxygen through a permeable membrane reactor. One side of the membrane is exposed to gas in the tubular catalyst bed, while the other side is exposed to air. The difference of oxygen partial pressures between the adjacent sides due to oxidation reaction in the catalyst bed causes oxygen to permeate from the airside to the catalyst bed through the membrane by ionic and electronic diffusion mechanism. This can provide uniform oxygen distribution and better control for the process in addition to higher concentration of hydrogen in the product gas as air nitrogen is abandoned in the supply feed using the membrane.

Axial mass dispersion is found to have a negligible effect on the concentration profiles. This is an expected result as the L/d_p ratio used in investigating the reactor operation is 200, which is much higher than the Carberry criterion ($L/d_p > 50$). The axial thermal dispersion, however, slightly influences the temperature behavior along the reactor. Fig. 7 shows the steady state temperature profiles along the axial direction of the reformer in the two cases of presence and absence of the heat axial dispersion term in the model. Neglecting the axial dispersion of heat generates an axial shift in the local temperatures varying along the front part of the reactor. At the first 4% of the axial direction, the shift is 11.8 °C, at 10% of the length the shift is 2.63 °C, while it results in an offset of −2.75 °C in temperature in the rear part of the reformer.

The influence of the S/C and O/C molar ratios on the ATR performance is presented in Figs. 8 and 9 in terms of CH_4 conversion, thermal reforming efficiency, and H_2 purity obtained

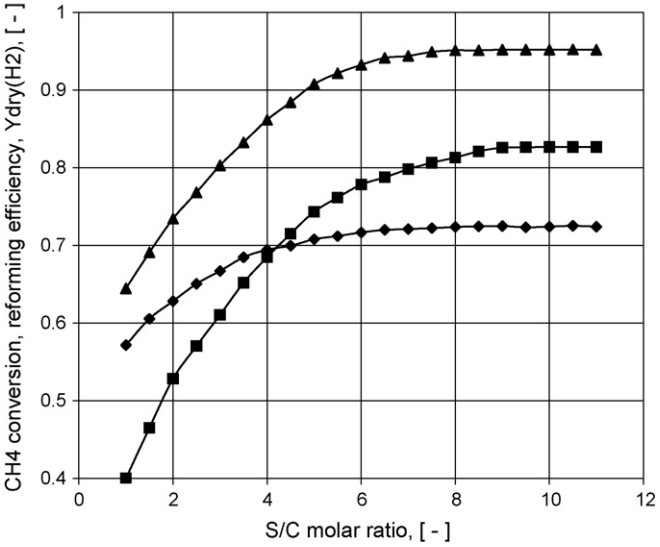

Fig. 8. Effect of S/C ratio on ATR performance, at 500 °C, 1.5 bar, O/C = 0.45. (■) Reformer efficiency; (▲) CH_4 conversion; (♦) Y_{dry}, (H_2).

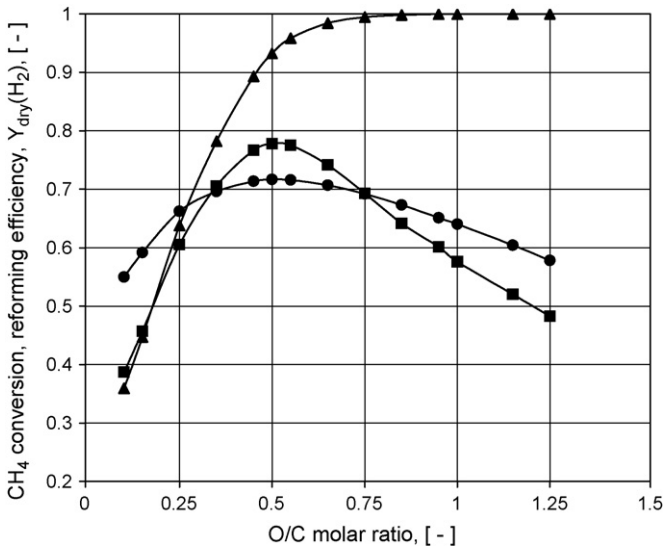

Fig. 9. Effect of O/C ratio on ATR performance, at 500 °C, 1.5 bar, S/C = 6. (▲) CH_4 conversion; (■) reformer efficiency; (●) Y_{dry}, (H_2).

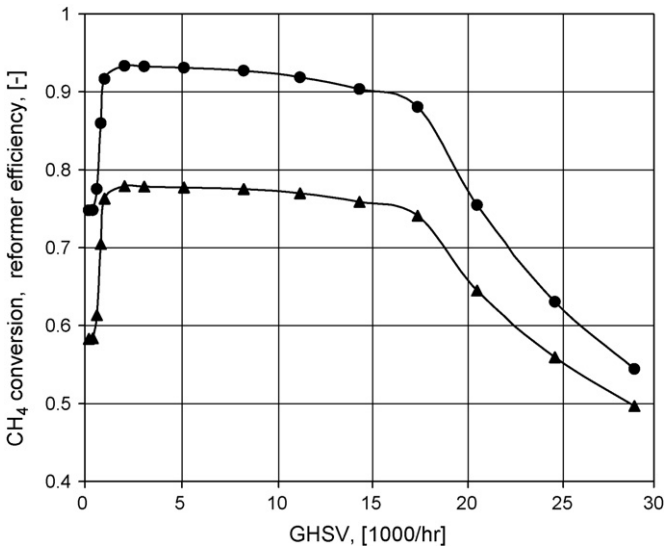

Fig. 10. Effect of GHSV on ATR performance, at 500 °C, 1.5 bar, O/C = 0.5, S/C = 6. (●) CH_4 conversion; (▲) reformer efficiency.

on dry basis. Fig. 8 shows the S/C ratio versus conversion, efficiency, and H_2 purity at fixed O/C ratio of 0.45 and at a pressure of 1.5 bar. Apparently, there is a maximum or saturation value for the ratio of steam that can be mixed with the fuel in the reformer in order to enhance its behavior. Beyond a ratio of S/C of 6, there is no further increase in the dry basis H_2 composition (73%) and CH_4 conversion (93%). There is still a little increase in the amount of H_2 produced per mole of CH_4 fed to the reformer and consequently in the thermal efficiency of the unit, which can reach about 83% at high load of steam (S/C ratio).

This, however, means more economic burden on the process in terms of raw material operational costs, and construction costs of a bigger reformer, and therefore might not make it a promising alternative. Thus the optimal operational window for the steam load (S/C ratio) can be taken as 4.5–6.0 where a fuel conversion of 90–93%, an H_2 purity of 70–73%, and a thermal efficiency of 71.5–78% can be realized.

Fig. 9 shows a local optimal window for oxygen load (O/C ratio) to the reformer of 0.45–0.55 on molar basis at a fixed S/C ratio of 6 that can produce a maximum H_2 purity of 73% and a thermal efficiency of 78%, and naturally a yield of 2.59 H_2 produced per mole of CH_4 fed. However, the fuel conversion is always favored by a high O/C ratio, but on the balance of low H_2 selectivity because most of the CH_4 in this case will be consumed via the oxidation reaction to CO_2.

Fig. 10 gives a relatively wide window of operation for the gas feed flow velocity through the reformer from which an improved ATR performance in terms of fuel conversion and thermal efficiency can be attained. A GHSV in the range of 204.8–28,664 h^{-1}, corresponding to a residence time of 17.6–0.12 s, is investigated at fixed ratios of O/C and S/C of 0.5 and 6, respectively. It can be seen that at a low gas flow velocity, meaning a high residence time of the species in the reactor, the conversion obtained is as low as 74.8% and the thermal efficiency is around 58%.

This is an expected result due to the fact that at low gas flow velocity, the mass transport between the bulk gas and the catalyst surface is certainly a limiting factor. Thus, low production rates and conversion levels are obtained. On the other hand at very high gas feed velocity (very short residence times through the reactor), there is indeed not enough time for the reactions to provide sufficient conversion or to reach equilibrium compositions. However, a relatively wide regime of space velocities (1050–14,000 h^{-1}) can provide optimal values for conversion and efficiency around 93 and 78%, respectively. The process at this plateau can be recognized as a kinetically limited process, where the internal kinetic limitations are controlling.

5. Conclusions

The ATR process performance in terms of fuel conversion, reforming efficiency, and H_2 purity and yield is demonstrated in a fixed bed reformer of 0.4 m in length using a 1-D heterogeneous reactor model. The reformer temperature and product gas composition are directly affected by the operating ratios of S/C and O/C in the feed, in addition to feed temperature and residence time along the catalyst bed. Unsuitable feed composition, i.e. high oxygen partial pressure (corresponding to an O/C ratio greater than 0.45) at high-pressure operation (greater than 4.5 bar), can generate serious hot-spot formation at the catalyst surface. High-pressure operation will lower the fuel conversion and demands high steam loads (S/C ratio). Improved performance of the ATR is determined to provide up to 93% methane conversion, reformer efficiency of 78%, H_2 yield and purity of 2.6 and 73%, respectively, using an O/C ratio of 0.45, an S/C ratio of 6, a feed temperature of 500 °C, a pressure of 1.5 bar, and a GHSV of 3071 h^{-1}. An optimal window of operation is given in Table 8. The gas and catalyst temperatures are shown to have good proximity with only 11 °C difference within the first 10% of the reformer front and 89 °C above feed tem-

Table 8
Summary of optimal operational conditions for the ATR process

Performance criteria				
Fuel conversion (%)	Thermal reforming efficiency (%)		Hydrogen yield	Hydrogen purity (%)
93	78		2.6	73
Optimal operational parameters				
GHSV (h^{-1})	O/C molar ratio	S/C molar ratio	Temperature (°C)	Pressure (bar)
1050–14,000	0.45–0.55	4.5–6.0	500	1.5

perature at the aforementioned operational conditions. Steady state conditions are reached in about 13 min. The ATR process is kinetically limited with the catalyst properties investigated here.

Acknowledgments

The financial support of SenterNovem under project no. 10002820 is gratefully acknowledged and the collaboration with the Energy Research Center of The Netherlands (ECN) is highly appreciated.

References

[1] S. Ahmed, M. Krumpelt, Hydrogen from hydrocarbon fuels for fuel cells, Int. J. Hydrogen Energy 26 (2001) 291–301.
[2] P.M. Biesheuvel, G.J. Kramer, Two-section model for autothermal reforming of methane to synthesis gas, AIChE J. 49 (2003) 1827–1837.
[3] L. Barreto, A. Makihira, K. Riahi, The hydrogen economy in the 21st century: a sustainable development scenario, Int. J. Hydrogen Energy 28 (2003) 267–284.
[4] H.D. Lee, D.V. Applegate, S. Ahmed, S.G. Calderone, T.L. Harvey, Hydrogen from natural gas: part I—autothermal reforming in an integrated fuel processor, Int. J. Hydrogen Energy 30 (2005) 829–842.
[5] B.C.R. Ewan, R.W.K. Allen, A figure merit assessment of the routes to hydrogen, Int. J. Hydrogen Energy 30 (2005) 809–819.
[6] J.N. Armor, Catalysis and the hydrogen economy, Catal. Lett. 101 (2005) 131–135.
[7] I. Dybkjaer, Tubular reforming and autothermal reforming of natural gas—an overview of available processes, Fuel Process. Technol. 42 (1995) 85–107.
[8] S.S. Bharadwaj, L.D. Schmidt, Catalytic partial oxidation of natural gas to syngas, Fuel Process. Technol. 42 (1995) 109–127.
[9] L. Ma, D.L. Trimm, Alternative catalyst bed configurations for the autothermic conversion of methane to hydrogen, Appl. Catal. A 138 (1996) 265–273.
[10] M.A. Pena, J.P. Gomez, J.L.G. Fierro, New catalytic routes for syngas and hydrogen, Appl. Catal. A 144 (1996) 7–57.
[11] K. Aasberg-Petersen, T.S. Christensen, C.S. Nielsen, I. Dybkjaer, Recent developments in autothermal reforming and pre-reforming for synthesis gas production in GTL applications, Fuel Process. Technol. 83 (2003) 253–261.
[12] A. Heinzel, B. Vogel, P. Hubner, Reforming of natural gas—hydrogen generation for small scale stationary fuel cell systems, J. Power Sources 105 (2002) 202–207.
[13] L. Mleczko, M. Baerns, Catalytic oxidative coupling of methane—reaction engineering aspects and process schemes, Fuel Process. Technol. 42 (1995) 217–248.
[14] E.H. Stitt, Multifunctional reactor? 'Up to a point lord copper', Chem. Eng. Res. Des. 82 (2004) 129–139.
[15] S.H. Chan, H.M. Wang, Thermodynamic analysis of natural gas fuel processing for fuel cell applications, Int. J. Hydrogen Energy 25 (2000) 441–449.
[16] S.H. Chan, H.M. Wang, Effect of natural gas composition on autothermal fuel reforming products, Fuel Process. Technol. 64 (2000) 21–39.
[17] S.H. Chan, H.M. Wang, Carbon monoxide yield in natural gas autothermal reforming process, J. Power Sources 101 (2001) 188–195.
[18] D.L. Hoang, S.H. Chan, Modeling of a catalytic autothermal methane reformer for fuel cell applications, Appl. Catal. A 268 (2004) 207–216.
[19] J. Xu, G.F. Froment, Methane steam reforming, methanation and water–gas shift: I. intrinsic kinetics, AIChE. J. 35 (1989) 88–96.
[20] G. Xiu, P. Li, A. Rodrigues, Sorption enhanced reaction process with reactive regeneration, Chem. Eng. Sci. 57 (2002) 3893–3908.
[21] D.L. Trimm, C.-W. Lam, The combustion of methane on platinum-alumina fibre catalysts—I. Kinetics and mechanism, Chem. Eng. Sci. 35 (1980) 1405–1413.
[22] C.R.H. De Smet, M.H.J.M. de Croon, R.J. Berger, G.B. Marin, J.C. Schouten, Design of adiabatic fixed-bed reactors for the partial oxidation of methane to synthesis gas. Application to production of methanol and hydrogen-for-fuel-cells, Chem. Eng. Sci. 56 (2001) 4849–4861.
[23] A.M. De Groote, G.F. Froment, Simulation of the catalytic partial oxidation of methane to synthesis gas, Appl. Catal. A 138 (1996) 245–264.
[24] A.M. De Groote, G.F. Froment, Th. Kobylinski, Synthesis gas production from natural gas in a fixed bed reactor with reversed flow, Can. J. Chem. Eng. 74 (1996) 735–742.
[25] K. Gosiewski, U. Bartmann, M. Moszczynski, L. Mleczko, Effect of intraparticle transport limitations on temperature profiles and catalytic performance of the reverse-flow reactor for the partial oxidation of methane to synthesis gas, Chem. Eng. Sci. 54 (1999) 4589–4602.
[26] G.F. Froment, K.B. Bischoff, Chemical Reactor Analysis and Design, Wiley, London, 1990.
[27] S. Ergun, Fluid flow through packed columns, Chem. Eng. Prog. 48 (1952) 89–94.
[28] M.F. Edwards, J.F. Richardson, Gas dispersion in packed beds, Chem. Eng. Sci. 23 (1968) 109–123.
[29] S. Yagi, D. Kunii, N. Wakao, Studies on axial effective thermal conductivities in packed beds, AIChE J. 6 (1960) 543–546.
[30] D. Kunii, J.M. Smith, Heat transfer characteristics of porous rocks, AIChE J. 6 (1960) 71–78.
[31] A.P. De Wash, G.F. Froment, Heat transfer in packed bed, Chem. Eng. Sci. 27 (1972) 567–576.
[32] C.H. Li, B.A. Finlayson, Heat transfer in packed bed—a reevaluation, Chem. Eng. Sci. 32 (1977) 1055–1066.
[33] N. Wakao, S. Kaguei, Heat and Mass Transfer in Packed Bed, Gordon and Breach, New York, 1982.
[34] R.C. Reid, J.M. Prausnitz, B.E. Poling, The Properties of Gases and Liquids, McGraw-Hill, New York, 1988.
[35] R.B. Bird, W.E. Stewart, E.N. Lightfoot, Transport Phenomena, second ed., Wiley, New York, 2002.
[36] C.J. Geankoplis, Transport Processes and Unit Operations, third ed., Prentice Hall Int., 1993.
[37] Y. Ding, E. Alpay, Adsorption-enhanced steam–methane reforming, Chem. Eng. Sci. 55 (2000) 3929–3940.

[38] D. Dissanayake, M.P. Rosynek, K.C.C. Kharas, J.H. Lunsford, Partial oxidation of methane to CO and H_2 over a Ni/Al_2O_3 catalyst, J. Catal. 132 (1991) 117–127.

[39] L. Ma, D.L. Trimm, C. Jiang, The design and testing of an autothermal reactor for the conversion of light hydrocarbons to hydrogen. I. The kinetics of the catalytic oxidation of light hydrocarbons, Appl. Catal. A 138 (1996) 275–283.

[40] D.L. Hoang, S.H. Chan, Effect of reactor dimensions on the performance of an O_2 pump integrated partial oxidation reformer—a modelling approach, Int. J. Hydrogen Energy 31 (2006) 1–12.